JOURNAL OF MATERIALS SCIENCE 4 (1969) 544–553

Low Endurance Fatigue in Metals and Polymers

Part 3 *The Mechanisms of Failure*

B. TOMKINS*, W. D. BIGGS
Engineering Laboratory, University of Cambridge, UK

Submitted 14 December 1967 and accepted 25 February 1969

Studies of crack growth in fatigue of annealed aluminium, Nylon 66 and Araldite epoxy resin have revealed two mechanisms, shear and tensile tearing. The former applies both to fatigue and to tensile straining under approximately plane strain conditions and requires a capacity for plastic flow within the material. The latter mechanism occurs where flow is either restricted or impossible. A model for crack propagation in low endurance fatigue is described, and a rigid-plastic analysis is shown to be consistent with the observations.

1. Introduction

In a previous paper [1] the phenomenological relationships between stress range, strain range and cycles were examined for the low endurance ($< 10^4$ cycles) fatigue of aluminium, Nylon 66 and an Araldite epoxy resin. Such relationships do not, however, give information about the mechanisms of failure. Even at low applied strains cracks are formed within the first few per cent of the life [2] and, in the low endurance range, most of the life is spent in crack propagation.

In all but extremely thin sheet specimens (or in specimens containing long cracks) crack propagation is, approximately, a process of plane strain, and the direction of growth is perpendicular to the plane of the sheet. In the usual type of push-pull fatigue specimen, crack growth occurs in this way. The present paper examines this mechanism, under high applied strains, by means of direct observation on specially shaped specimens and by fractographic study of the surfaces produced by the tests described in [1].

2. Previous Work on Fatigue Crack Propagation at High Strains

2.1. Metals

In studies of high-strain torsional fatigue in brass Wood *et al* [3] placed emphasis on block substructure formation and crack initiation ahead of the main crack front. The main crack was propagated by the linking up of microcracks by plastic tearing. From observations on the fracture surfaces of aluminium alloys, Forsyth [4] proposed two mechanisms of crack growth: Stage I, operative in the early stages, was governed by the maximum shear stress and the crack propagated from surface intrusions along a plane of maximum shear. When the crack had propagated a short distance this was succeeded by Stage II, which was governed by the maximum principal tensile stress, causing the crack to propagate in a direction normal to this stress. Following Stage II growth the fracture surface was covered with ripple markings delineating successive arrests of the crack front, suggesting that ripple formation was dependent on separation by plastic flow at the crack tip.

Laird and Smith [5] observed both stages in pure aluminium and nickel. In the low endurance range, 95% of the fracture surface of aluminium was produced by Stage II growth. They suggested a plastic separation process in which the crack tip was successively blunted and resharpened during each cycle. In a later paper [6] they observed that, at high strains, cracks initiated

*Now at UKAEA (Reactor Group), Springfields, Lancs, UK.

quickly at the surface by plastic instability rather than by slip band intrusion.

2.2 Polymers

Early theories attributed fatigue failure to general structural disintegration due to molecular bond rupture and sliding [7]. More recently, failure in many polymers has been associated with crack initiation and propagation as in metals. Prevorsek and Lyons [8] found this to occur in Nylon 66 fibres. Ripple formation has been observed on the fracture surfaces of a strain-crystallising rubber [9] and a crystalline polycarbonate resin [10]. Lake and Lindley [11] observed slow, stable crack growth in many rubbers and proposed that the rate of crack growth is controlled by a modified Griffith criterion.

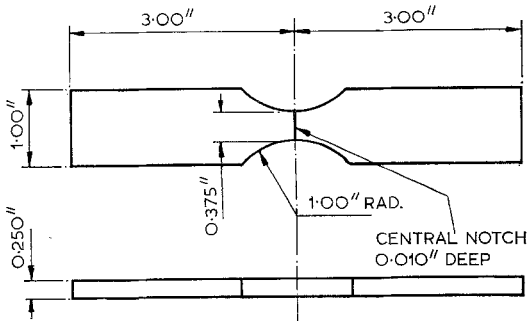

Figure 1 Crack propagation specimen.

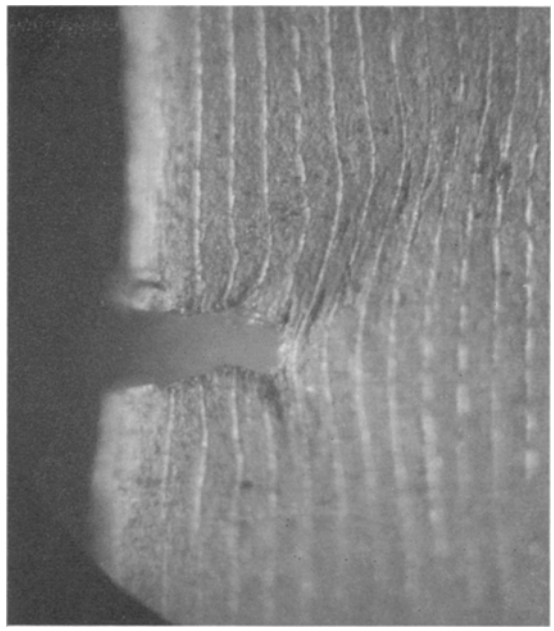

Figure 2 Aluminium crack tip region during propagation (× 38). $N_f = 30$ cycles.

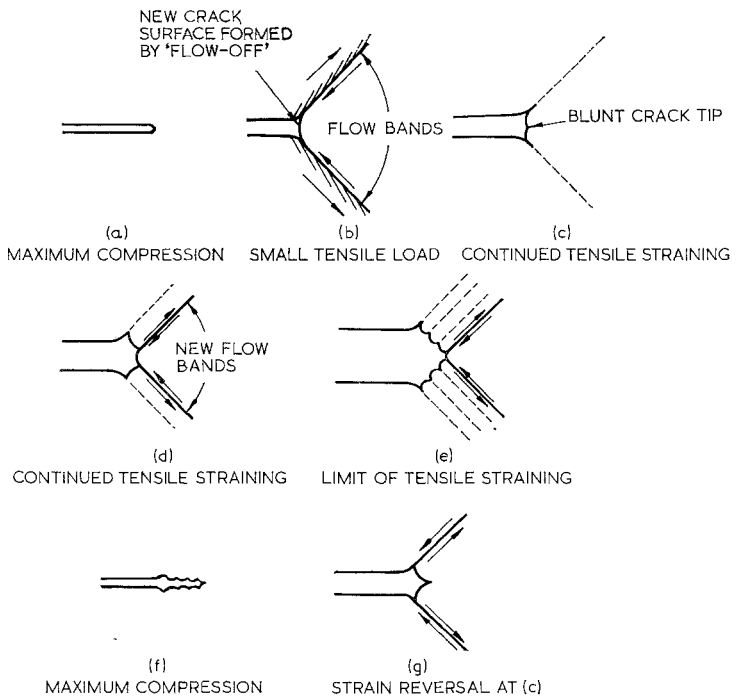

Figure 3 Stage II crack propagation process in aluminium.

3. Experimental Procedure

While it is impossible to obtain truly plane strain conditions at the surface, it is possible to minimise and to mask plane stress effects by observing the edge of a thick specimen as a crack propagates across the thickness. If the applied strains are sufficiently high the internal plastic deformation around the crack tip controls most of the deformation occurring at the surface. Fig. 1 shows the specimens used; they were waisted at the centre to prevent instability in compression and contained a central notch on one side to initiate the crack. Testing was under push-pull conditions using fixed limits of strain; all tests were of less than 500 cycles duration so that all internal crack growth occurred in a direction perpendicular to the maximum tensile stress. The crack tip was observed at magnifications up to $\times$ 40; in some cases a parallel grid was scribed on the surface as shown in fig. 2. Some specimens were sectioned and the internal deformation (as revealed by the deformation of the grains) was compared with the surface observations. In all cases the agreement was good suggesting that plane stress effects were minimal.

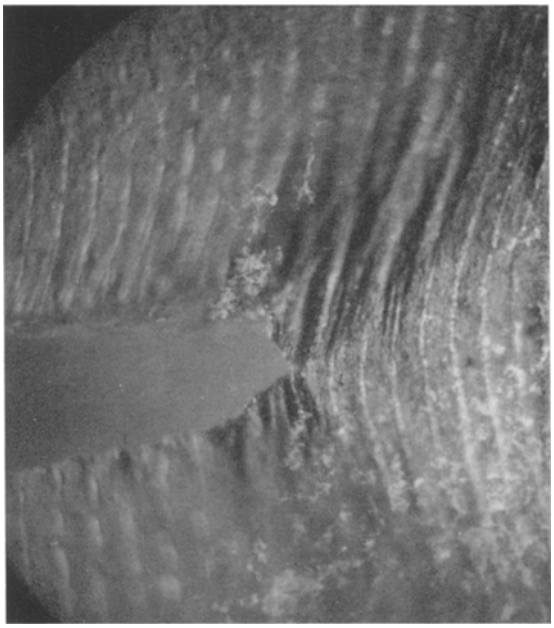

Figure 4 Aluminium crack tip at maximum tensile strain ($\times$ 38). $N_f = 30$ cycles.

4. Direct Observations

4.1. Aluminium

Within the first few cycles localised plastic shear could be detected on two planes radiating from the notch root at $\pm$ 45° to the tensile axis; a visible crack then developed from the notch and shear flow from the crack tip on two similar planes became extensive; the material outside the two flow bands was relatively undistorted (fig. 2). Hardness tests showed a significant increase in hardness along the flow bands close to the crack tip and decreasing with distance from the tip. The hardness just ahead of the tip and between the flow planes was low and comparable with that at points well removed from the flow planes.

The process of crack propagation is summarised schematically in fig. 3. Under maximum compression (a) the crack tip was sharp but, on reversing the load, the crack began to propagate soon after a mean tensile stress was obtained. Plastic flow occurred on the 45° planes and new crack surface was formed by "flow-off" to produce a blunted crack tip with "ears" (b). Further straining in tension caused "flow-off" to stop at the edges of the initial flow planes due, presumably, to considerable strain hardening. Fracture occurs at the centre of the blunted crack (c) followed by further relaxation and crack growth on new flow bands at 45° to this point (d). This process is repeated until the maximum tensile strain is reached when the crack tip is as shown in (e) and in fig. 4.

Reversal of the strain causes the flow bands to operate in the opposite direction and the final geometry at maximum compression is shown in (f). If repeated this process produces Stage II cracking. If the strain is reversed from tension at a time when the tip is blunted (as in (c)), new, reverse flow occurs along the bands as in (g) to produce a sharpening of the crack tip. This process was observed as "folding over" of the tip by Laird and Smith [5].

Figs. 5a to d indicate that a similar process occurs under continuous tensile loading where the various stages of initial flow (a), notch blunting (b), inward spreading of the flow bands towards the notch centre (c) and fracture spreading by "flow-off" may be recognised.

The process of crack extension in fatigue appears therefore, to be a localised form of tensile fracture from a notch. It is worth noting that, in a tensile test of an un-notched ductile metal, this "flow-off" occurs in the sides of the "cup" after the internal crack has formed by void

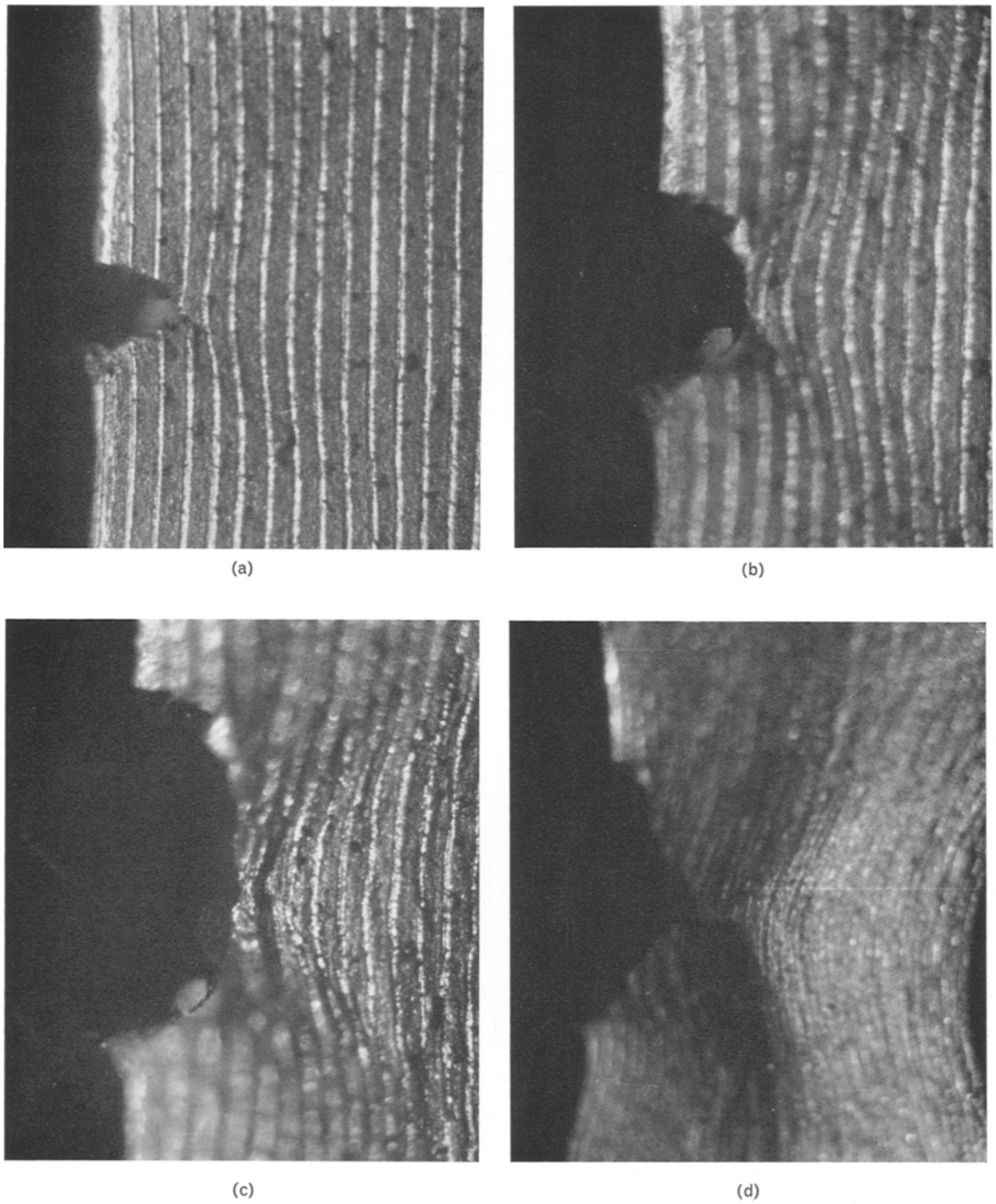

Figure 5 (a–d) Progress of failure in notched tensile test on aluminium. (Δ = crosshead deflection). (a), $\Delta = 0.068$ in. (× 36); (b), $\Delta = 0.108$ in. (× 36); (c), $\Delta = 0.146$ in. (× 32); (d), $\Delta = 0.206$ in. (× 12).

coalescence, whereas in high strain fatigue an external crack is nucleated by repeated slip. In either case, once a large enough crack has been formed, propagation is by Stage II growth.

4.2. Araldite

Relatively little deformation occurred around the crack tip, and that which did occur was of a viscous nature causing blunting. Since the three

dimensional network structure of Araldite precludes deformation by slip no flow bands were observed at 45°, and strain relief at the crack tip occurred by microcracking with accompanying viscous flow. At the limit of tensile straining the crack tip geometry was different from that observed in aluminium (fig. 6).

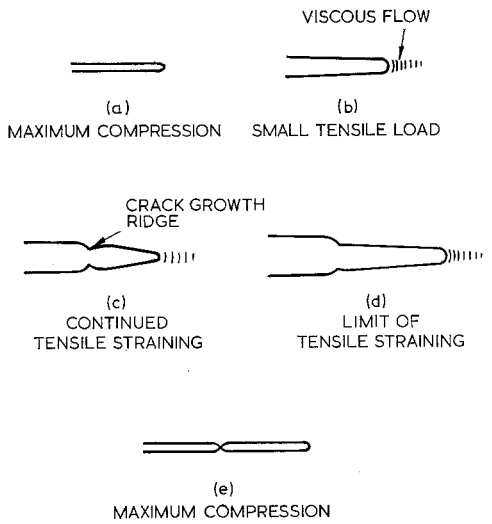

Figure 6 Crack propagation process in Araldite.

This process of tensile tearing was time-dependent; growth of the crack continued under a constant tensile strain. Thus it would be expected that crack growth would be dependent on the cycling frequency, being slower at higher frequencies as was, in fact, observed [1].

The fracture of a notched tensile specimen occurred by a similar process.

4.3. Nylon

Nylon 66 failed, in fatigue, by a combination of the shear flow and tensile tearing modes. Some shear deformation occurred along the planes of maximum shear (fig. 7) and produced a limited amount of new crack surface by "flow-off". However, the applied strains were generally too high for all the crack deformation to be accommodated in this way and some tensile tearing occurred. For the same reason most of the fractures in notched tensile tests occurred by tearing, the mechanism being similar to that observed in the fatigue tests.

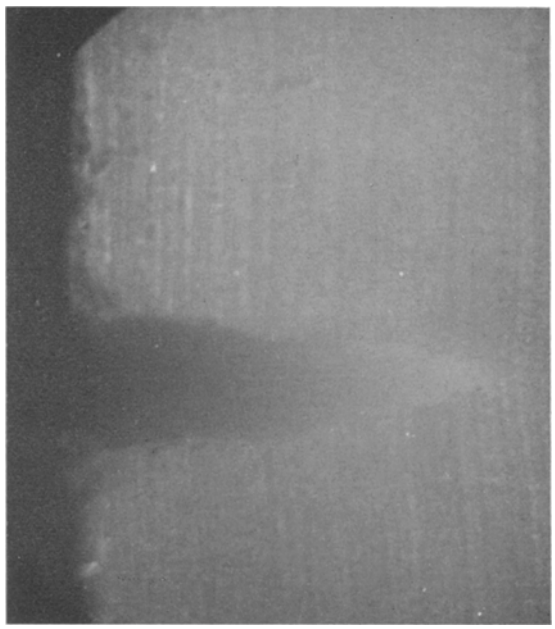

Figure 7 Deformation in region of nylon crack tip (× 17.5). $N_f = 80$ cycles.

5. Fractography

Since the experimental arrangements for direct observation were only satisfactory for tests at high strains (generally < 100 cycles) a fractographic study was made of all specimens in order to cover endurances up to 5×10^4 cycles. A scanning electron microscope was used.

5.1. Aluminium

The fracture surfaces show the features expected from the Stage II type flow mechanism of fig. 3. At lower strains the deformation at the crack tip could be wholly accommodated by the initial "flow-off" producing a single ripple (as a deep valley); these were observed on the higher endurance specimens. At higher strains each ripple is succeeded by finer striations—these are shallower valleys formed by intermediate "flow-off" (fig. 8). Both ripples and striations are continuous, indicating steady crack growth during a cycle. Heavily deformed ridges parallel to the direction of crack growth (fig. 9) indicate a boundary between growth on different levels perpendicular to the tensile axis.

The size of the ripples varied considerably, from 1 to 300 μm wide depending on the applied strain. Striations were always about 1 μm wide, suggesting that Stage II fracture operates on an

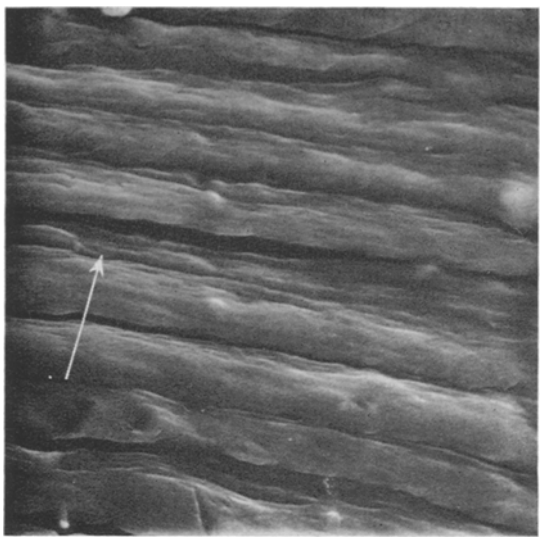

Figure 8 Ripples and striations on aluminium fracture surface (× 1648). N_f = 460 cycles; arrow shows direction of crack growth.

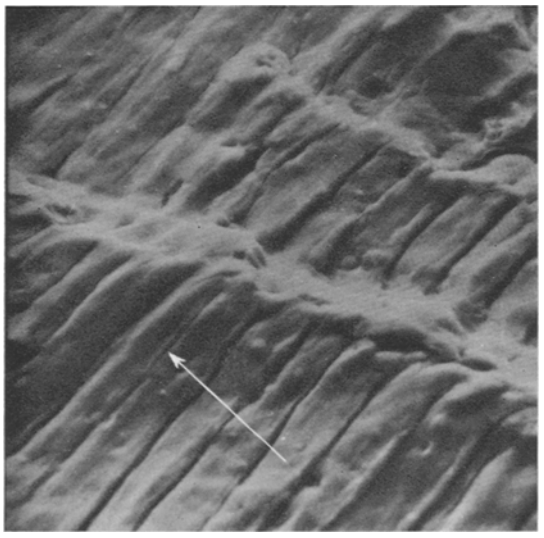

Figure 9 Aluminium fracture surface (× 815). N_f = 1950 cycles; arrow shows direction of crack growth.

extremely fine scale and must involve some minute microplastic fracture.

Fractography of the notched tensile specimens showed continuous striations, of width about 1 μm, perpendicular to the direction of crack growth. Similar observations have been made by McClintock [12] and Rogers [13].

5.2. Araldite

Fractographic observations supported the mechanism proposed in fig. 6. The fractures were all perpendicular to the tensile axis and showed a pattern of shallow parallel ridges which increased in width with increased applied strain at a given frequency. Broutman and McGarry [14] observed similar ridges on the tensile fracture surface of a polyester-styrene resin when fracture occurred by discontinuous crack growth. Tear lines radiated from the crack source in a direction perpendicular to the main crack front; these indicate crack advance on different levels (cf. the ridges on the fractures of aluminium).

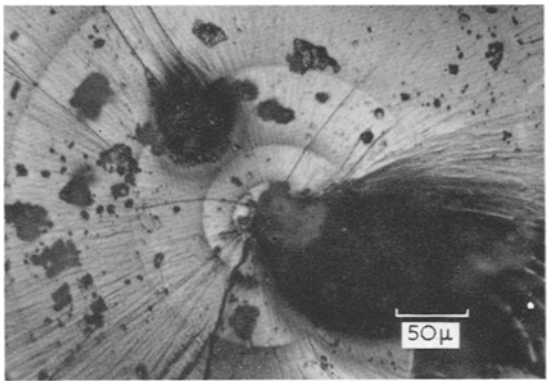

Figure 10 Araldite fracture surface: crack growth from internal defect (× 193). N_f = 6 cycles.

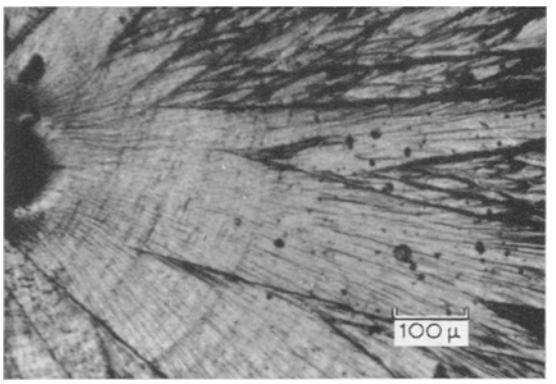

Figure 11 Araldite fracture surface: low strain crack growth from external defect (× 96). N_f = 32 000 cycles.

At high applied strains, cracks initiated on the first cycle from an internal defect (fig. 10) and grew concentrically, indicating Griffith-type

growth involving minimisation of surface energy. At lower strains cracking was initiated at an external defect and fig. 11 shows a "mirror zone" around the source before the coarser tear lines become apparent. This "mirror zone" is attributed [15] to slow crack growth and was not found in the tensile fractures. The tensile fractures did, however, show the parabolic traces which characterise microcracking ahead of the main crack; no such markings were found on the fatigue fractures.

5.3. Nylon

The nylon fractures showed both shear and tensile tearing, the extent of each depending on the magnitude of the applied strain. At low strains, fracture occurred by shear flow only and the surface was covered by ripples which were continuous but shallow, consistent with the reduced capacity of the material to deform by shear (fig. 12). Ripple widths down to about 4 μm were observed. At high strains (< 100 cycles endurance) an increasing proportion of the surface showed tear lines and fine, discontinuous striations (fig. 13). At very high strains cracks generally initiated at internal defects and parabolic markings indicated advance microcracking.

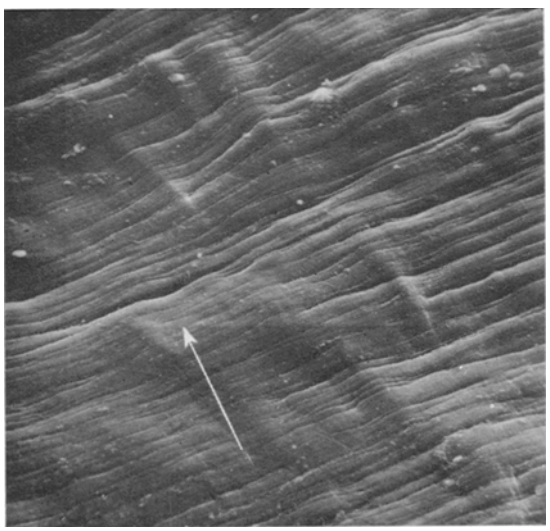

Figure 12 Ripples and striations on nylon fracture surface (× 336). $N_f = 19\,000$ cycles; arrow shows direction of crack growth.

Fractures produced by tensile straining showed evidence of considerable advance microcracking, final fracture occurred by the linking of many internal microcracks to yield a rough fracture

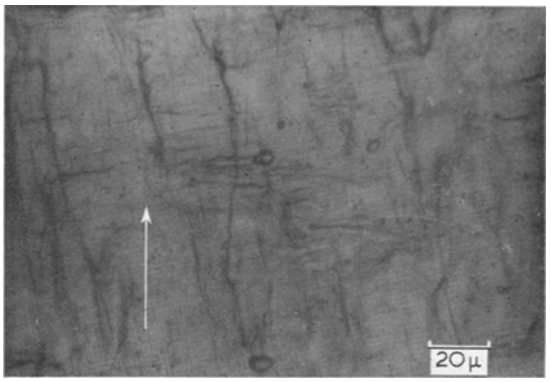

Figure 13 Tear lines and discontinuous striations on nylon fracture surface (× 386). $N_f = 71$ cycles; arrow shows direction of crack growth.

surface. The small capacity for plastic flow causes blunting of the microcracks so that the growth of any single crack is inhibited, leading to a high tensile strength. Cyclic loading at high strains probably helps the growth of internal microcracks thus producing the combination of features observed.

6. Discussion

The shear mechanism described in fig. 3 (Stage II crack growth) is very similar to the idealised non-cumulative plane strain tensile fracture model proposed by Cottrell [16] in which a plane strain crack spreads by the injection of edge dislocations into the material along the shear planes at 45° to the crack tip. Under cyclic loading this occurs during the tension stroke. Subsequent reversal alters the direction of flow and, since the crack tip does not weld up, dislocation injection begins again at the new crack tip when tension is reapplied. According to this model new crack surface is not formed on all operative flow planes but only on the plane at the inner edge of the flow band where the shear strain gradient is greatest. Kraft and Hertzberg [17] have observed this "flow-off" process along the line of maximum shear strain gradient in tensile fracture studies of a Cu–Cr alloy.

The observation that Stage II fracture in aluminium occurs on the planes of maximum shear suggests that the essential difference between Forsyth's Stage I growth (at 45° to the metal surface) and Stage II growth is that, in the former case, only one shear plane is operative at the crack tip whereas, in Stage II both planes operate. Thus we expect a continuity in fatigue behaviour from high strain (primarily Stage II

cracking) to low strain (primarily Stage I) if the majority of the fatigue life is concerned with crack propagation.

Since it appears that shear, and not tensile strains are primarily responsible for all new crack surface it is evident that the amount and direction of crack growth per cycle ("flow-off") is controlled solely by the magnitude and direction of the zones of high deformation (flow bands) which exist at the crack tip. These are, in turn, controlled by the applied strain and hence, for strain cycling, the rate of crack growth should be controlled by the magnitude, and not by the frequency, of straining. This has been shown to be true for aluminium and nylon over the range of frequencies used [1]. It is also worth noting that de Villiers [18] has shown that the shear mechanism also operates when the external loading system is multiaxial: tests on mild steel in both pure shear and equi-biaxial loading have shown that fracture occurs by this mechanism.

When shear flow is restricted (as in nylon at high strains) or impossible (as in Araldite at all strains) relaxation at the crack tip occurs by tensile tearing. In this case the crack usually initiates from material defects. At high strains, where high triaxial stresses exist along the tensile axis, cracking was initiated on the axis but, at lower strains, the size of the initial defect may be expected to have an effect on the endurance since it is probably more difficult to initiate a crack from a small defect. In the present tests a moderate-sized defect (usually an air bubble) was always present.

The presence of continuous tear lines across the fracture surfaces indicates that strain reversal simply halts the continued propagation of the crack. The increase in the spacing of the crack arrest ridges when the specimen was cycled at a lower frequency for a given strain range indicates that the crack is only quasi-stable, and if the specimen be held under a constant tensile strain the crack continues to propagate. For polymers in which viscous flow is even more restricted fatigue crack propagation will also be restricted because the cracks would soon become unstable.

7. Crack Propagation in Fatigue

The basic failure criterion governing fatigue failure in many metals is the Coffin-Manson law relating plastic strain range and endurance by a simple power function. Since the shear mechanism of crack growth is dependent upon the extent of plastic flow ahead of the crack it is reasonable that the endurance (the sum of crack growth over the number of cycles to failure) should be a a function of the applied plastic strain range. Tomkins [19] has recently analysed the shear mechanism quantitatively and has shown that it predicts the Coffin-Manson law.

The relationship between plastic strain range and endurance for the three materials tested is repeated in fig. 14. For aluminium the shear mechanism operates and the Coffin-Manson law applies whereas in nylon, the shear mechanism is only dominant for endurances greater than 100 cycles. Here again the Coffin-Manson law applies.

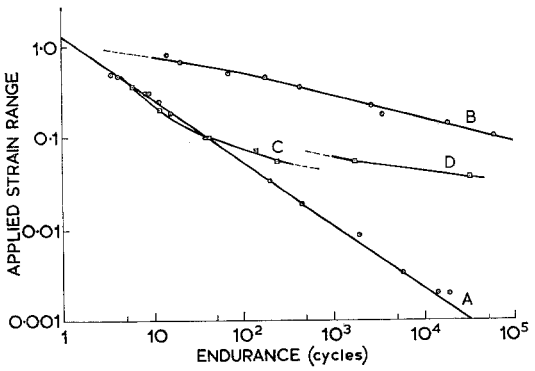

Figure 14 Applied strain range versus endurance.
A, aluminium (plastic strain range) 5 c/m and 300 c/m.
B, Nylon 66 (total strain range) 5 c/m and 300 c/m.
C, Araldite (total strain range) 5 c/m.
D, Araldite (total strain range) 300 c/m.

Crack growth under the tensile tearing criterion is controlled by the applied stress rather than by the applied strain, and deviations from the Coffin-Manson law arise in nylon for endurances less than 100 cycles, and in Araldite.

The effect of cycling frequency is also shown. The shear mechanism is independent of frequency whereas the tensile mechanism is greatly affected, the crack growth per cycle being reduced at higher frequencies.

8. Conclusions

(i) Failure by shear occurs in both tensile and fatigue straining under plane strain conditions. It requires a capacity for shear flow in the material and is controlled by the strain (or the strain gradient) on planes of maximum shear radiating from the crack tip.

(ii) Where shear flow is restricted or impossible, failure in both tension and fatigue occurs by tensile tearing. It is controlled by the maximum tensile stress at the crack tip.

Acknowledgements

The authors wish to acknowledge the assistance of Mr R. Brand in obtaining the experimental results. Laboratory facilities and equipment were provided by Professor Sir John F. Baker. One of the authors (B.T.) is indebted to the Science Research Council for financial support.

Appendix

Distribution of Strain at the Tip of a Crack

Theoretical

As gross plastic flow occurs in the region of the tip of a fatigue crack it is useful to derive the strain distribution around a crack in a rigid-plastic body. Lee* has derived the slip line field for a V-notched bar pulled in tension; as the notch angle becomes zero the system approximates to a crack. The upper half of a slip line field for a plane strain crack (OC) under tensile strain is shown in fig. A1.

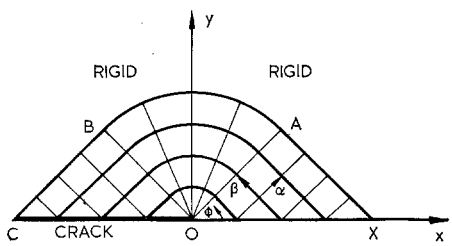

Figure A1 Rigid – plastic model, slip line field.

To consider the velocity field, the upper and lower parts of the specimen are given unit velocity. The material on OX is then stationary. Superposing a unit upwards velocity on the system brings the material below the crack to rest and the material on OX now has unit vertical component of velocity. The slip line velocity relations are,

$$\left.\begin{aligned} du - v\,d\phi &= 0 \text{ on } \alpha \text{ lines} \\ dv + u\,d\phi &= 0 \text{ on } \beta \text{ lines} \end{aligned}\right\} \quad \text{(A1)}$$

where u and v are the velocity components along α and β lines respectively.

Since all α lines are straight and the rigid material below the lower half of the slip line field is at rest

$$u = 0 \quad \text{(A2)}$$

Hence, from (A1), v is constant and, as unit velocity is produced on OX,

$$v = \sqrt{2} \quad \text{(A3)}$$

Now the strain rates of the slip line field can be determined by the relations

$$\left.\begin{aligned} \dot{\epsilon}_x &= \frac{\partial \dot{u}_x}{\partial x} \\ \dot{\epsilon}_y &= \frac{\partial \dot{v}_y}{\partial y} \\ \dot{\epsilon}_{xy} &= \left(\frac{\partial \dot{u}_x}{\partial y} + \frac{\partial \dot{v}_y}{\partial x}\right) \end{aligned}\right\} \quad \text{(A4)}$$

where $\dot{u}_x$ and $\dot{v}_y$ are the displacement rate components in the x and y directions and are given by

$$\left.\begin{aligned} \dot{u}_x &= -v\sin\phi \\ \dot{v}_y &= v\cos\phi \end{aligned}\right\} \quad \text{(A5)}$$

In the regions COB and XOA ϕ is constant and hence

$$\dot{\epsilon}_x = \dot{\epsilon}_y = \dot{\epsilon}_{xy} = 0$$

but in the region AOB, from (A4) and (A5)

$$\left.\begin{aligned} \dot{\epsilon}_x &= -\dot{\epsilon}_y = \frac{v}{x}\sin\phi\cos^2\phi \\ \dot{\epsilon}_{xy} &= -\frac{v}{x}\cos\phi\cos 2\phi \end{aligned}\right\} \quad \text{(A7)}$$

and from (A7) the maximum shear strain rate ($\dot{\gamma}_{max}$) is

$$\dot{\gamma}_{max} = \frac{v}{2x}\cos\phi\,(1 + 3\cos^2 2\phi)^{\frac{1}{2}} \quad \text{(A8)}$$

Fig. A2 shows the variation of $\dot{\gamma}_{max}$ with ϕ. The maximum value of $\dot{\gamma}_{max}$ occurs at $\phi = \pi/4$ and the direction of $\dot{\gamma}_{max}$ is along OA. The distribution of $\dot{\gamma}_{max}$ along OA is given by

$$\dot{\gamma}_{max} = \frac{v}{2\sqrt{2x}} \quad \text{(A9)}$$

i.e. it is inversely proportional to the distance along OA.

Thus, according to the rigid-plastic model, the maximum values of shear strain and shear strain gradient occur on lines at $\pm 45°$ and in the direction of these lines. It is interesting to note that $\dot{\gamma}_{max}$ is almost at the maximum value

*E. H. Lee, *J. Appl. Mech.* **19** 331.

between $\phi = \pi/4$ and $\pi/3$ so that high plastic strains can be expected in this region as was, in fact, observed.

Strain Measurement

Assuming that the lines at 45° to the crack tip underwent shear strain only fig. A2 can be analysed quantitatively and the shear strain distribution along the inner edge of the flow band can be determined. This distribution is shown in fig. A3. Away from the crack tip the shear strain is inversely proportional to the distance from the tip, thus confirming the theoretical prediction (equation A9). The similarity of tensile and fatigue distributions is also shown in the data taken from the notched tensile test of fig. 5b. Close to the crack tip a deviation from the inverse relationship between strain and distance occurs; in this region the strain attains a fairly uniform maximum value.

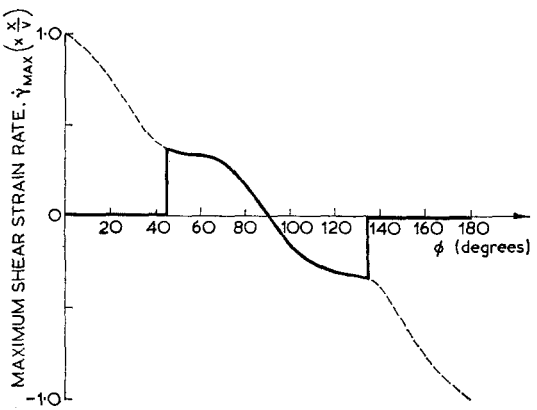

Figure A2 Maximum shear strain rate versus angle ϕ.

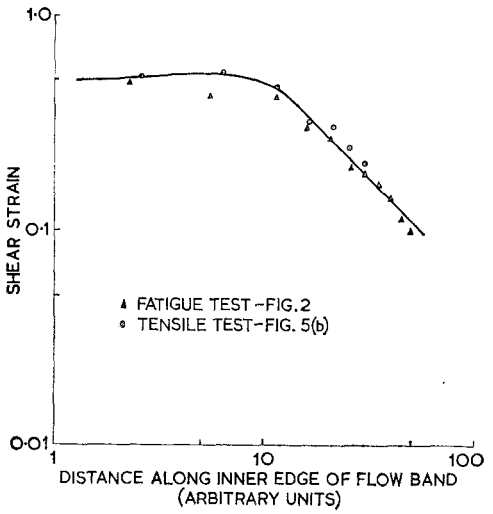

Figure A3 Distribution of shear strain along inner edge of flow band.

References

1. B. TOMKINS and W. D. BIGGS, *J. Materials Sci.* **4** (1969) 000.
2. N. THOMPSON, "Fracture", edited by Averbach (Technology Press, 1959) p. 354.
3. W. A. WOOD, S. COUSLAND, and K. R. SARGENT, *Acta Metallurgica* **11** (1963) 643.
4. P. J. E. FORSYTH, Symp. on Crack Propagation, Cranfield (1961) p. 76.
5. C. LAIRD and G. C. SMITH, *Phil. Mag.* 7 (1962) 847.
6. *Idem, ibid* **8** (1963) 1945.
7. W. F. BUSSE *et al*, *J. Appl. Phys.* **13** (1942) 715.
8. D. PREVORSEK and W. J. LYONS, *ibid* **35** (1964) 4152.
9. E. H. ANDREWS, *ibid* **32** (1961) 542.
10. A. J. MCEVILY, R. C. BOETTNER, and T. L. JOHNSTON, "Fatigue", 10th Sagamore Conf. (Syracuse University Press, 1964) p. 95.
11. G. J. LAKE and P. B. LINDLEY, Conf. on Physical Basis of Yield and Fracture (Inst. Phys. and Phys. Soc. 1966) p. 176.
12. F. A. MCCLINTOCK, as ref. [2] p. 560.
13. H. C. ROGERS, as ref [2] p. 46.
14. L. J. BROUTMAN and F. J. MCGARRY, *J. Appl. Polymer Sci.* **9** (1959) 609.
15. I. WOLCOCK and S. B. NEWMAN, "Fracture Processes in Polymeric Solids," edited by Rosen (Interscience, 1964) p. 235.
16. A. H. COTTRELL, as ref [4] p. 1.
17. R. W. KRAFT and R. W. HERTZBERG, *Trans AIMME* **227** (1963) 580.
18. J. W. R. DE VILLIERS, Ph.D Thesis (University of Cambridge, 1966).
19. B. TOMKINS, *Phil. Mag.* **18** (1968) 1041.